sustainability

MDPI

Article

Demand Response Management of a Residential Microgrid Using Chaotic Aquila Optimization

Sushmita Kujur [1], Hari Mohan Dubey [1] and Surender Reddy Salkuti [2,*]

[1] Department of Electrical Engineering, BIT Sindri, Dhanbad 828123, India
[2] Department of Railroad and Electrical Engineering, Woosong University, Daejeon 34606, Republic of Korea
* Correspondence: surender@wsu.ac.kr

Abstract: In this paper, Chaotic Aquila Optimization has been proposed for the solution of the demand response program of a grid-connected residential microgrid (GCRMG) system. Here, the main objective is to optimize the scheduling pattern of connected appliances of the building such that overall user cost are minimized under the dynamic price rate of electricity. The GCRMG model considered for analysis is equipped with a fuel cell, combined heat and power (CHP), and a battery storage system. It has to control and schedule the thermostatically controlled deferrable and interruptible appliances of the building optimally. A multipowered residential microgrid system with distinct load demand for appliances and dynamic electricity price makes the objective function complex and highly constrained in nature, which is difficult to solve efficiently. For the solution of such a complex highly constrained optimization problem, both Chaotic Aquila Optimization (CAO) and Aquila optimization (AO) algorithms are implemented, and their performance is analyzed separately. Obtained simulation results in terms of optimal load scheduling and corresponding user cost reveal the better searching and constrained handling capability of AO. In addition, experimental results show that a sinusoidal map significantly improves the performances of AO. Comparison of results with other reported methods are also made, which supports the claim of superiority of the proposed approach.

Keywords: smart grid; residential microgrid; demand response; appliances scheduling; Aquila optimization; sinusoidal map

Citation: Kujur, S.; Dubey, H.M.; Salkuti, S.R. Demand Response Management of a Residential Microgrid Using Chaotic Aquila Optimization. *Sustainability* **2023**, *15*, 1484. https://doi.org/10.3390/su15021484

Academic Editors: Seyed Masoud Mohseni-Bonab, Ali Moeini and Ali Hajebrahimi

Received: 27 November 2022
Revised: 31 December 2022
Accepted: 5 January 2023
Published: 12 January 2023

1. Introduction

Power systems nowadays are facing various challenges such as fossil energy consumption on a large scale, increased carbon emissions, and the growing importance of energy and environmental issues. Therefore, a shift towards a reliable, effective, and sustainable energy system has become the current requirement. Smart Grids are being deployed worldwide due to their ability to improve the efficiency, dependability, and security of the power system [1]. This knits together a multidisciplinary approach such as multiple energy resources, sophisticated sensors and automated metering for control, two-way communications, intelligent electrical distribution equipment, and cutting-edge computing systems [2]. All the above technology together helps to respond to changes in electric demand and provides benefits to both suppliers and consumers such as integration of renewable energy resources (RES), increase in the reliability of operation, help in reducing operation and maintenance costs for the utilities, and also provision of real-time information to consumers about their power consumption pattern that helps them to shuffle their load as per tariff. The change in electricity consumption patterns by consumers that helps the utility to balance supply and demand is known as demand response (DR) [3]. DR can provide secured operation and reduce the need for investment in inefficient peaking power plants through load curtailment and shifting. It can provide consumers with time-varying prices of electricity and incentives to ensure the economical and efficient use of energy. Moreover,

the DR program helps to enhance the reliability of the power system, and therefore, the consumer obtains the advantage of more stable power with lower outages [4]. However, uncertainty associated with RES, social, economic, and environmental impact needs to be investigated.

The challenges of DR programs include the absence of suitable market mechanisms in the existing market structures. The need to maintain the safety of the system is subtly transferred from the utility to the end-user by switching to a system in which price adaptive demand is used to deliver various system functions. For DR modeling generally, the following assumptions are taken into consideration: its economically rational behavior, aggregated demand with different load types, and in-depth system and demand knowledge [5]. DR programs can be applied to residential, commercial, and industrial sectors. They are categorized into two types: (i) incentive-based, where the customers receive incentives for altering their consumption habits under supply-side demands, and (ii) price-based, in which the cost of electricity supply is taxed at various rates depending on when they use electricity [6]. In recent years, researchers have shown their interest in DR, and they have published various articles.

1.1. Literature Review

Several research works have been conducted with one or more objectives among the following: minimization of operation cost, minimization of carbon emissions, minimization of the electric bill of consumers, maximizing the profit of system operator, reliability of the overall system, etc. The impact of the operational cost incurred with and without coordination of different distributed energy resources (DER) is investigated using PSO [7]. It helps to make proper tariff arrangements under the above two scenarios of DER arrangements. Optimum generation scheduling of a grid-connected microgrid system equipped with solar PV system, wind, and diesel generator is carried out in [8,9]. Here, incentive-based DR is incorporated to maximize operator benefit. DR maximizes the profit of the operator and also facilitates consumers by an incentive for controlling their load during peak load time [10,11]. A fair comparison under two scenarios, i.e., with and without implementation of DR for a MG system, was made, which shows the significant probability of energy saving through DR as it also helps to curtail the electric bill of consumers.

The DR program helps to optimize power generation costs by shifting energy consumption patterns and the possible reduction of load by the consumer, whereas rescheduling different DER as per day ahead load demand helps to reduce the generation cost for the operator. In Reference [12], the DR program has been implemented on a grid-connected 33-bus system comprised of RES. The simulation analysis carried out in the paper claims that a significant reduction in network power loss and hence increase in the profit of operators can be achieved by it. A multiperiod optimal power flow approach is investigated on IEEE 9 and IEEE 118 bus systems using linear programming. Here, it was observed that the DR program in the network helps to provide a cost-effective solution and also improves the voltage stability of the system [13]. A residential microgrid system is a complex network since it combines different energy resources, and energy storage systems to fulfill the required load demand of various loads of appliances of building premises. For this Incentive based DR (IBDR) was applied to enhance reliability. IBDR was found to be effective in reducing the overall operational cost of microgrids [14–16]. In Reference [17] IBDR with one selling price among two industrial consumers was analyzed with variation in discomfort weight factor. Here, also IBDR was found to be effective in solving demand deficit issues.

A day-ahead dynamic price-based DR modal was proposed with the operation of microturbines with uncertain RES on an hourly basis to maximize the economic benefit [18,19]. This model was found to be effective in achieving higher profits with lower voltage deviation than the conventional strategy. Moreover, proper scheduling of load helps to reduce the size of DER, improves the load factor of the whole system [20], and is able to maintain the balance between supply and demand efficiently [21,22]. Cogeneration refers to the

simultaneous production of thermal and electric energy from a single source. This helps to reduce carbon emissions and cost of energy and also improves the overall efficiency of the system [23]. A grid-connected home energy system, which combines fuel cell (FC) with combined heat and power, and a battery storage system (BSS) have been considered for optimal scheduling. Analysis was carried out under two different scenarios ((i) without BSS with fixed tariff and (ii) with BSS and dynamic tariff [24]), combining FC and Gas turbine plants with combined heat and power (CHP) [25] and using a grid-connected hybrid PV with storage [26]. Simulation results carried out under different operational constraints show that optimal scheduling of thermal and electric generation significantly reduces the overall operational cost.

The high share of integrated RES contributes more economical benefits, reduces greenhouse emissions from the environment, and provides better energy security. To analyze the economic and environmental benefits, a DR program was conducted on the residential MG system [27–31], CHP-based reconfigurable MG system [32], demand response analysis framework with multiple BSS [33], and CHP-based MG with multiple markets [34]. The cost of the MG emitted emission and the demand cost are optimized simultaneously by linear programming. The ε-constraints method is used to solve multi-objective (MO) problems whereas the scenario generation and reduction approach was used as a tool to handle uncertainty associated with RES [34]. MO scheduling for a CHP-based MG tied with compressed air energy storage has been carried out using the ε-constraints method [27]. To find out the optimal solution, the fuzzy decision approach was used, showing that it helps to reduce operating costs and emissions significantly.

For a grid-connected residential MG that knits together RES and BSS, NGSA III was used to minimize consumption cost, inconvenience cost, and pollution [28]. The impact of using biomass and seawater electrolyzers on operational costs and emitted greenhouse emissions for residential MG systems empowered by RES and hydrogen power has been investigated under different cases [29]. Here, it was observed that biomass integration helps to reduce operating costs whereas FC integrated with seawater electrolyzer reduces emissions significantly. A new demand response analytical framework (DRAF) was analyzed in a python environment for (i) DR in the production process, (ii) design optimization of battery with a PV system, and (iii) DR of distributed thermal energy resources. It was observed that using Pareto front through Price based DR, cost and emissions are reduced [33].

A critical review in the area of DR problems can be found in [4–6,35,36]. Moreover, the chronological framework of the work carried out in the area of DR with the objective and applied solution methodology is presented in Table 1 below.

Table 1. Chronological framework in the area of DR.

Year/Reference No.	Method	Objective	Grid	Wind	PV	ESS	EV	FC
2010 [7]	PSO with stochastic repulsion	Maximization of user benefit	√	×	√	×	√	×
2014 [24]	CCA	Operating cost Minimization	√	×	×	√	×	√
2015 [18]	HSS	Operating cost minimization	√	×	×	√	×	√
2016 [30]	CPLEX, PSO	Operating cost minimization	√	×	×	√	×	×
2017 [19]	TSRO, MILP solved by GUROBI, C&CG	Operating cost minimization	√	√	√	×	×	×
2017 [21]	MILP solved using GUROBI.	Operating cost minimization, Peak load reduction	√	×	√	√	×	CHP
2017 [8]	GTDR using AIMMS	Fuel cost minimization, Utility benefit maximization	√	√	√	×	×	×
2018 [26]	GA	Operating cost minimization	√	×	√	√	×	CHP
2018 [37]	MILP & Greedy method	Operating cost minimization	√	√	√	√	√	×

Table 1. *Cont.*

Year/Reference No.	Method	Objective	Grid	Wind	PV	ESS	EV	FC
2019 [14]	Hybrid price-based DR program	Maximize profit, minimize consumer cost	√	√	√	×	×	×
2019 [34]	LP with augmented $\varepsilon-$constraint	Operating cost minimization and pollution minimization	√	√	√	√	×	CHP
2020 [15]	IBDR, Monte-Carlo	Operating cost minimization	√	×	√	√	×	×
2020 [28]	NSGA-III	Operating cost, inconvenience cost, and pollution minimization	√	√	√	√	√	√
2020 [25]	ABC	Operating cost minimization	√	×	×	×	×	√
2020 [31]	MINLP, PSO, gradient-based deterministic approach	Operating cost minimization	√	×	×	√	×	√
2021 [27]	RTP-based DR program	Operating cost minimization	√	√	√	√	×	×
2021 [12]	PSO, (2m + 1) point estimation	Minimization of fuel cost, and grid power cost, Maximization of profit for MG operator	√	√	√	×	×	×
2021 [10]	GA	Operating cost minimization, maximizing stability	√	×	√	√	×	×
2021 [32]	$\varepsilon-$constraint, fuzzy decision making	Operating cost and emission minimization,	√	√	×	√	×	CHP
2022 [11]	linear regression, PSO.	Profit maximization	√	√	√	×	×	×
2022 [22]	Hybrid Jaya-IPM	Operating cost minimization	×	√	√	√	×	×

Designing an efficient DR program for an efficient energy management system is very difficult due to its complex structure. These complexities arise due to the uncertainty of DER, the unpredictable pattern of energy consumption, and complicated connected appliance loads. For the solution of such a highly complex constrained optimization problem, researchers have applied various analytical as well as nature-inspired (NI) algorithms until now. Among the analytical approaches, game theory [8], linear programming (LP) [11,13,34], Monte-Carlo simulation [15], and mixed integer nonlinear programming (MINLP) [31,33,34] were used to solve this problem.. The NI algorithms include particle swarm optimization (PSO) [7,17], grey wolf optimizer [9], Genetic Algorithm (GA) [10,26], Jaya algorithm [22], Artificial Bee Colony Algorithm (ABC) [26], and NSGA-III [28]. The NI technique is found to be very effective for the solution of nonlinear, discontinuous, and multi-modal functions, and it mostly provides a reasonable solution efficiently [38,39].

Energy management in the residential sector is very important as connected appliances in it consume the major part of the power generated by the energy sector. Here, the primary function is to minimize the operational cost associated with fulfilling the demand for the connected appliances in the building. Therefore, designing an effective DR model for it with the complicated operational constraints and an effective solution is a difficult task. It needs a robust optimization technique to solve such type of complex constrained optimization problem. The "no free lunch theorem" states that no algorithm can guarantee to solve all types of optimization problems, as there is always a chance for improvement in it [40]. Keeping this statement in mind, Aquila Optimization embedded with a sinusoidal map is proposed to solve the DR model of a GCRMG system.

Aquila Optimization (AO) belongs to the family of NI algorithms, developed by Abualigah et al. in 2021 [41]. Since its beginnings, it was implemented to reduce harmonic from the H Bridge inverter [42], for wind potential estimation [43], and for the solution

of industrial engineering optimization problems [44]. To the author's best knowledge, it is not implemented to solve energy management problems with the DR program to date. Moreover, AO is very easy to implement and has few control parameters.

1.2. Contribution

The main contribution in the paper is as follows:

DR model for a grid-connected residential microgrid (GCRMG) system has been developed in a MATLAB environment.

- For practical modeling of GCRMG, fuel cells, combined heat and power (CHP), and battery storage system (BSS) are also considered here.
- Chaotic Aquila Optimization (CAO) has been proposed for the solution of the DR model for the GCRMG system. Here, the objective is to analyze the optimal scheduling pattern of connected thermal and electric appliances such that overall user costs get minimized.
- The above system is analyzed by implementing CAO and AO individually.
- Finally, to prove the efficacy of the proposed CAO, a comparison of the results in terms of user cost is made with the result of AO and reported results by PSO [30], hybrid CONOPT, and PSO [31].

The remaining section of the paper is presented as given below.

Section 2 describes the required problem formulation. Section 3 presents a brief description of AO and the implementation process of a sinusoidal map in it. Section 4 presents the problem description simulation findings, while Section 5 offers concluding observations.

2. Problem Formulation

The primary function of an energy management system is to minimize the cost of operation while fulfilling all related constraints for the proper operation. The residential model considered here is powered through the grid, fuel cell, and battery storage system as shown in Figure 1. A micro-CHP using a fuel cell has also been utilized in this study. The load for the following model consists of a thermostatically controlled appliance, interruptible appliances, and deferrable appliances. Energy demand and resource operation must be coordinated to reduce the cost of daily energy usage [31].

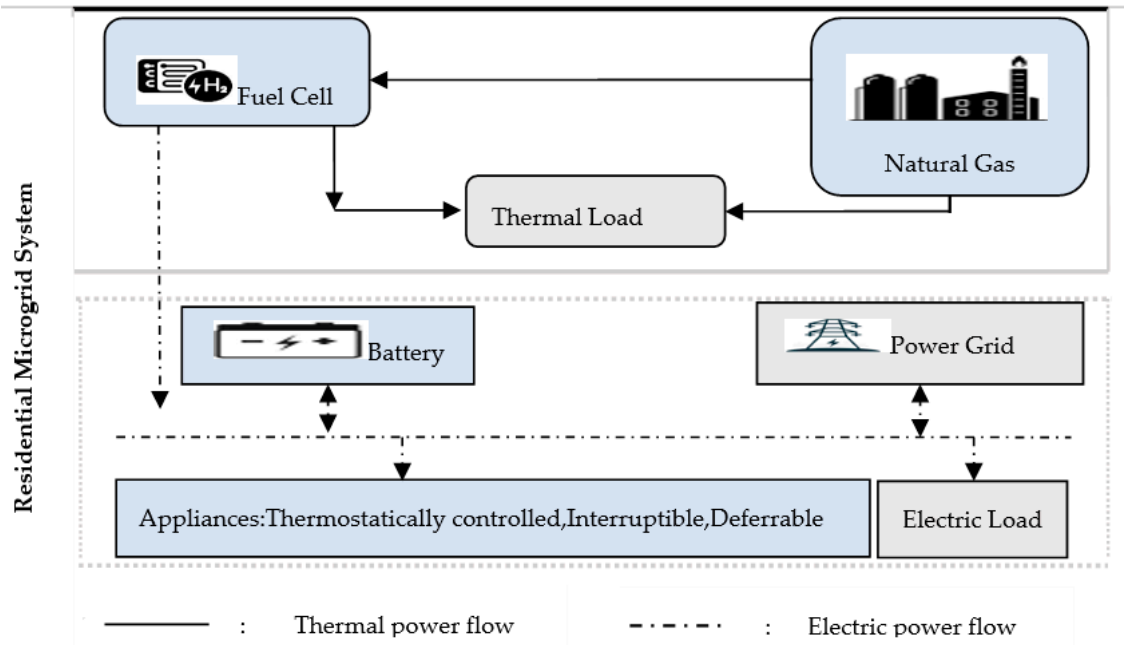

Figure 1. Residential Microgrid System.

2.1. Objective Function

The objective function that must be minimized can be formulated as follows [31]:

$$F_{min} = \sum_{h=1}^{24} [T_{elec}(h) * p_{grid}(h) + T_{gas} * p_{gas}(h) + T_{gas} * P_{FC}(h)] \quad (1)$$

where F_{min} is the total cost for 24 h. Here, h = (1,2 … 24), which is the time step and represents the 24 h in a day. $T_{elec}(h)$ is the hourly electricity price in RMB, and $p_{grid}(h)$ represents the quantity of power traded with the utility grid at hour h. The cost of natural gas is denoted by T_{gas}, and heat power generated by natural gas is denoted by $p_{gas}(h)$, and $P_{FC}(h)$ is the total power of the fuel cell.

2.2. Operational Constraints

2.2.1. Electrical Demand–Supply Balance

The electrical power supplied through the grid, battery, and fuel cell has to be equal to the total electrical demand of the residential building described below.

$$p_{grid}(h) + p_{batt}(h) + p_{eFC}(h) = p_{ms}(h) + p_{td}(h) + p_{defe}(h) + p_{inte}(h) \quad (2)$$

where $p_{grid}(h)$ is the grid power exchange, $p_{batt}(h)$ is the power supplied by the battery, and $p_{eFC}(h)$ is the electrical power of the fuel cell. The total energy used by unscheduled, must-run electrical appliances is represented by $p_{ms}(h)$. The power usage of a thermostatically controlled appliance is represented by $p_{td}(h)$ while $p_{defe}(h)$ and $p_{inte}(h)$ denote power consumed by deferrable electrical appliances and interruptible appliances over one hour, respectively.

2.2.2. Thermal Demand–Supply Balance

The thermal demand–supply balance can be represented by Equation (3) as below:

$$p_{gas}(h) + P_{hFC}(h) = P_{hms}(h) \quad (3)$$

where $P_{gas}(h)$ is the heat power generated by natural gas, and $P_{hFC}(h)$ is the heat power generated by the fuel cell. $P_{hms}(h)$ is the total thermal consumption.

2.2.3. Constraints for Battery Operation

A battery can operate at either a charging or discharging state at any given time. The battery storage system is rated its minimum (SOC^{min}) and maximum (SOC^{max}) range, to increase the lifespan; it should be operated in its specified range. The battery constraints are represented as [9],

$$0 \leq \frac{p_{batt}^{ch}(h)}{\eta_{ch}} \leq p_{ch}^{max} \quad (4)$$

$$0 \leq p_{batt}^{dch}(h) \times \eta_{dch} \leq p_{dch}^{max} \quad (5)$$

$$p_{batt}(h) = \frac{p_{batt}^{ch}(h)}{\eta_{ch}} - p_{batt}^{dch}(h) \times \eta_{dch} \quad (6)$$

$$SOC(h+1) = SOC(h) + \frac{p_{batt}^{ch}(h) - p_{batt}^{dch}(h)}{E_{batt}} \quad (7)$$

$$SOC^{min} \leq SOC(h) \leq SOC^{max} \quad (8)$$

where $p_{batt}^{ch}(h)$ is the charging power, and $p_{batt}^{dch}(h)$ is the discharging power of the battery at hour h, where as p_{ch}^{max} is the maximum charging power and p_{dch}^{max} is the maximum discharging power. $p_{batt}(h)$ denotes the output power of the battery, while η_{ch} and η_{dch} denote the charging and discharging efficiency. $SOC(h)$ represents the battery's state of charge at hour h, and E_{batt} represents the battery capacity. SOC^{min} and SOC^{max} are the rated minimum and rated maximum states of charge of the battery.

2.2.4. Constraints for the Appliance That Is Thermostatically Controlled

At each sub-interval, the thermostatically controlled appliance modifies its energy use to maintain the appropriate temperature. An air conditioner is used as a thermostatically controlled appliance in this study. The building's temperature at each hour is determined as in (9) given below [7]:

$$T_{in}(h+1) = T_{in}(h) * e^{\frac{-\Delta}{\tau}} + (R * P_{td}(h) + T_{out}(h)) * (1 - e^{\frac{-\Delta}{\tau}}) \quad (9)$$

where $\Delta = 1$ h and $\tau = RC$; $R = \frac{18^{\circ}\text{C}}{\text{kW}}$ and $C = 0.525$ kWh/°C.

The initial room temperature has been taken as 20 °C. The operational range and accompanying temperature range can be constrained by imposing the following restrictions:

$$T_{in}^{min} \leq T_{in}(h) \leq T_{in}^{max} \quad (10)$$

where T_{in}^{min} and T_{in}^{max} are the specified minimum and maximum indoor temperatures in °C.

2.2.5. Constraints for Interruptible Appliances

Interruptible appliances are supposed to operate in the "on" or "off" states in the desired time window of the consumer (α_a, β_b). If the appliance is turned on, it uses a fixed amount of energy during each sub-interval. As a result, the interruptible appliance's requirements can be expressed as follows [31]:

$$\delta_{a,t} = 0, t \notin [\alpha_a, \beta_b] \quad (11)$$

$$\sum_{t=\alpha_a}^{t_0-1} \delta_{a,t} + \delta_{a,t_0} + \sum_{\tau=t_0+1}^{\beta_a} \delta_{a,\tau} = H_a \quad (12)$$

$$\sum_{\tau=t_0+1}^{\beta_a} \delta_{a,t} = H_a \quad (13)$$

where $\delta_{a,t}$ denotes the state of the appliance "a" at the time (t) which is equal to "1", if the appliance is on and "0" if the appliance is off, and H_a represents time slots needed by appliance "a".

2.2.6. Deferrable Appliances Constraints

Unlike the previously stated interruptible appliance, the deferrable appliance should operate all the way through once it is started. Let H be the entire amount of time slots necessary for the deferrable appliance to operate at a particular level of energy. According to (14), the work should begin during the operational window $(\alpha_i, \alpha_i + \lambda_i)$. The non-interruptible property can be described using (15). The appliances should operate inside the operational window (α_a, β_b), according to (16).

$$\sum_{t=\alpha_i}^{t_0-1} \delta_{a,t} + \delta_{i,t_0} + \sum_{t=t_0+1}^{\alpha_i+\lambda_i} \delta_{i,\tau} \geq 1 \quad (14)$$

$$\sum_{\tau=t_0+1}^{t_0+H_i} \delta_{\tau} \geq H \times (\delta_{t_0+1} - \delta_{t_0}) \quad (15)$$

$$\sum_{t=\alpha_a}^{\beta_a} \delta_t = Ht\epsilon [\alpha_a, \beta_a] \quad (16)$$

where $\delta_{a,t}$ represents the on or off state of appliance "a" during time t in hours by either "1" or "0".

2.2.7. Constraints for Operation of a Fuel Cell

A fuel cell, which may simultaneously produce electrical and thermal energy, is an important component of the home energy management system. A fuel cell must therefore adhere to the following criteria.

$$P_{FC,h} - P_{FC,h-1} \leq \Delta P_{FC,U} \quad (17)$$

$$P_{FC,h-1} - P_{FC,h} \leq \Delta P_{FC,D} \tag{18}$$

$$P_{FC,min} \leq P_{FC} \leq P_{FC,max} \tag{19}$$

Here, $P_{FC,h}$ is the power of the fuel cell at hour h. $\Delta P_{FC,U}$ and $\Delta P_{FC,D}$ are the upper and lower limit of the ramp rate of the fuel cell. $P_{FC,min}$ and $P_{FC,max}$ are the minimum and maximum limits of fuel cell-generated power.

Part Load Ratio (PLR) influences the efficiency of a fuel cell and the electrical-to-thermal ratio and can be described as the ratio of electrical power produced by the fuel cell to its power rating [31]. The results below are feasible when $PLR_h \geq 0.05$:

$$\eta FC, h = 0.2716; \qquad \gamma FC,\ h = 0.6816 \tag{20}$$

If $PLR_h \leq 0.05$, then the equations given below can be used [31].

$$\eta FC, h = 0.9033PLR_h^5 - 2.9996PLR_h^4 + 3.6503PLR_h^3 - 2.0704PLR_h^2 + 0.4623PLR_h + 0.3747 \tag{21}$$

$$\gamma FC, h = 1.0785PLR_h^4 - 1.9739PLR_h^3 + 1.5005PLR_h^2 - 0.2817PLR_h \tag{22}$$

where $\eta FC, h$ represents the fuel cell's efficiency at hour h, and $\gamma FC,\ h$ is the ratio of the thermal energy produced by the fuel cell to its electrical energy.

3. Chaotic Aquila Optimization

3.1. Aquila Optimization

Aquila Optimization is an NI optimization algorithm influenced by the hunting behavior of Aquila found in nature. Aquila hunt for squirrels, rabbits, and various other creatures using their speed and razor-sharp talons. The Aquila employs four techniques while hunting prey. They are (i) selection of search area by high flight and vertical stoop, (ii) exploration within a narrow search space by contour flight along with short gliding attack, (iii) expanded exploitation by the low-flying descending attack within converge search space, and (iv) narrowed exploitation by swooping, walking and collecting prey. The mathematical model for hunting prey can be expressed in the following manner.

Firstly, a population of N no of candidate solutions is generated across a preset range using (23).

$$X_{i,j} = L_j + r \times (U_j - L_j) \tag{23}$$

where r is a random number between 0 and 1; $X_{i,j}$ is the j^{th} dimension of the i^{th} solution; L_j and U_j represents lower and upper bound values within the search space for the j^{th} dimension.

Expanded exploration is performed by Aquila by picking up the hunt location with a high soar and vertical stoop. It gives an estimate of the prey's location. Equation (24) is used to simulate this behavior and is carried out when $iter < \left(\frac{2}{3} \times MaxIter\right)$ and $r < 0.5$.

$$X_1(iter+1) = X_{best}(iter) \times \left(1 - \frac{iter}{MaxIter}\right) + (X_M(iter) - X_{best}(iter) \times r) \tag{24}$$

where $X_{best}(iter)$ represents the best solution till the current iteration. $X_M(iter)$ is the mean of the solutions available. $MaxIter$ is the maximum iteration, and $iter$ denotes the current iteration.

Contour flight and short gliding attack while performing narrowed exploration are simulated using (25).

$$X_2(iter+1) = X_{best}(iter) \times Levy(D) + X_R(iter) + (y - x) \times r \tag{25}$$

where $X_R(iter)$ is a randomly selected solution from the entire solutions, and $Levy(D)$ is the flight distribution function.

$$Levy(D) = s \times \frac{u \times \sigma}{\left| v^{\frac{1}{\beta}} \right|} \tag{26a}$$

$$\sigma = \left(\frac{\Gamma(1+\beta) \times \sin\left(\frac{\pi\beta}{2}\right)}{\Gamma\left(\frac{1+\beta}{2}\right) \times \beta \times 2^{\left(\frac{\beta-1}{2}\right)}}\right) \tag{26b}$$

The exploration process of search space in spiral shape is controlled using parameters x and y represented as below [41–44].

$$y = m \times \cos(\theta) \tag{26c}$$

$$x = m \times \sin(\theta) \tag{26d}$$

$$m = r_1 + U \times D_1 \tag{26e}$$

$$\theta = -\omega \times D_1 + \theta_1 \tag{26f}$$

$$\theta_1 = \frac{3 \times \pi}{2} \tag{26g}$$

were r_1 is the number of search cycle between 1 to 20; $U = 0.00565$; D_1 is the integers from 1 to the dimension of the search space length, and $\omega = 0.005$.

Expanded exploitation with a low-flying descending attack is performed by (27)

$$X_3(iter+1) = (X_{best}(iter) - X_M(iter)) \times \alpha - r + ((U - L) \times r + L) \times \delta \tag{27}$$

Here the parameters α and δ are set to 0.1.

The fourth method narrowed exploitation where the Aquila attacks by walking and grabbing prey are performed (28).

$$X_4(iter+1) = QF(iter) \times X_{best}(iter) - (G_1 \times X(iter) \times r) - G_2 \times Levy(D) + r \times G_1 \tag{28}$$

where QF represents a quality function, and the movements of the Aquila's prey are represented by G_1 and G_2.

$$QF(iter) = t^{\frac{2 \times r - 1}{(1 - MaxIter)^2}} \tag{29}$$

$$G_1 = 2 \times r - 1 \tag{30}$$

$$G_2 = 2 \times \left(1 - \frac{iter}{MaxIter}\right) \tag{31}$$

The continuous Aquila optimizer is transformed into its binary equivalent by converting each search agent's dimension to a probability value ranging from 0 to 1 by using (32)

$$S(X_i^d(iter+1)) = \frac{1}{1 + e^{-X_i^d(iter)/3}} \tag{32}$$

were,

$$X_i^d(iter+1) = \begin{cases} 1, & if\ rand \le S(X_i^d(iter+1)) \\ 0, & otherwise \end{cases} \tag{33}$$

3.2. Chaotic Aquila Optimization

Literature suggests that the chaotic sequence numbers generated by the strategy of chaotic map enhance the population diversity of the evolutionary algorithm, therefore, improving the global searching capability of the algorithm and avoiding the local op-

tima [45,46]. Keeping this in mind sinusoidal chaotic sequence (39) is introduced to replace random numbers of (24)–(28), and it is visualized over 100 iterations in Figure 2.

$$\mathcal{X}_{n+1} = a\mathcal{X}_n^2 \times Sin(\pi\mathcal{X}_n), \quad where \quad a = 2.3. \tag{34}$$

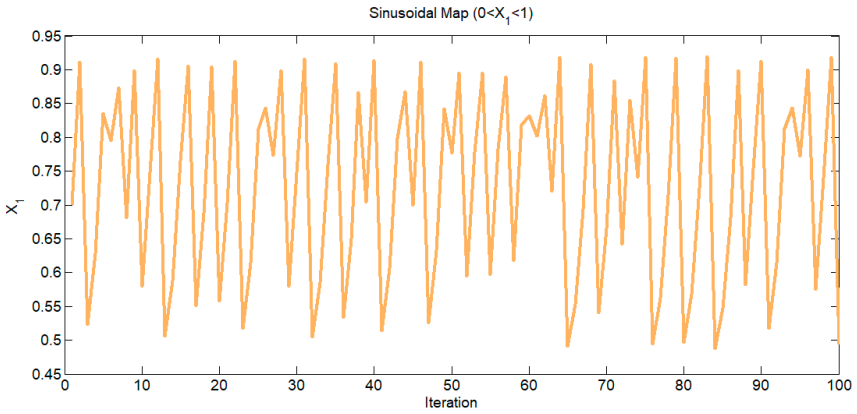

Figure 2. Visualization of Sinusoidal map.

The solution strategy used for finding the best solution using Chaotic Aquila Optimization (CAO) algorithm is presented in Section 3.3 and by the flowchart in Figure 3.

3.3. Implementation of CAO for the Solution of the Residential Microgrid Problem

The major steps associated with it are given below.

Step 1-N no of initial population is created for each variable for 24 h such as $P_{batt}\{1 \ldots 24\}$, $P_{FC}\{1 \ldots 24\}$, $P_{ta}\{1 \ldots 24\}$, $P_{gas}\{1 \ldots 24\}$, $P_{inte}\{1 \ldots 24\}$, $P_{defer}\{1 \ldots 24\}$ which represents the battery power, fuel cell power, thermal appliance power, thermal power supplied by natural gas, and the power consumed by interruptible and deferrable appliances. The fitness value of the population is evaluated and checked for all associated constraints.

Step 2-AO is applied to these variables of battery, fuel cell, and thermal appliance according to each exploration while CAO is applied to interruptible and deferrable appliances in each of the four exploration and exploitation stages using an equation.

- Expanded exploration:

$$X_1(iter+1) = X_{best}(iter) \times \left(1 - \frac{iter}{MaxIter}\right) + (X_M(iter) - X_{best}(iter) \times Ch_{ij}) \tag{35}$$

- Narrowed exploration:

$$X_2(iter+1) = X_{best}(iter) \times Levy(D) + X_R(iter) + (y - x) \times Ch_{ij} \tag{36}$$

- Expanded exploitation and low flying:

$$X_3(iter+1) = (X_{best}(iter) - X_M(iter)) \times \alpha - r + ((U - L) \times Ch_{ij} + L) \times \delta \tag{37}$$

- Narrowed exploitation where the Aquila attacks by walking and grabbing prey:

$$X_4(iter+1) = QF(iter) \times X_{best}(iter) - (G_1 \times X(iter) \times r) - G_2 \times Levy(D) + Ch_{ij} \times G_1 \tag{38}$$

Step 3-The new fitness function is calculated.

Step 4-It is then compared with the previous fitness function and updated if found better.

Step 5-Check if the iteration is reached termination criteria; if yes, then print the best fitness and its corresponding variables, otherwise repeat step 2.

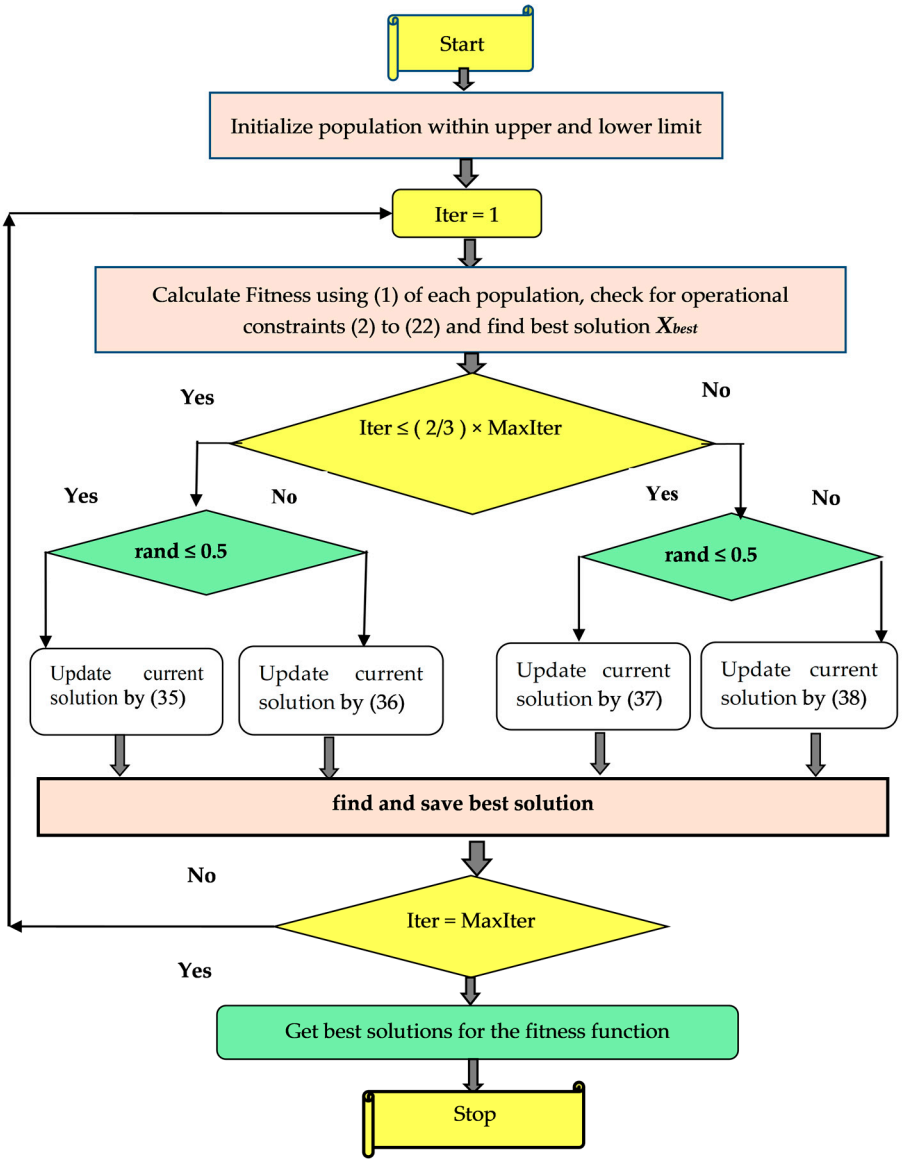

Figure 3. Flowchart for the solution of DR problem using CAO algorithm.

4. Simulation Analysis and Results

The DR model of a GCRMG system has been carried out for 24 h of a day. The DR model consists of a battery, fuel cell, thermal load, and deferrable and interruptible appliances. Additionally, for reliable and secure operation, the building also has a power supply from the grid. Here, it is assumed that the price of electricity is dynamic in nature where the price of electricity during peak hours is more as compared to during non-peak hours. Hence, optimal energy management of the combined system has been carried out such that load demand constraints are fully satisfied with minimum cost. The data for appliances (Interruptible and Deferrable), their power rating, the permissible operational interval during a day, and maximum operational time are listed in Table 2, whereas room temperature, parameters of the battery storage system, and fuel cell data are adopted similarly to Reference [31] and also listed in Table 3. The power demand, heat demands, and real-time electricity prices over different hours of the day are given in Table 4. Figure 4 shows the outdoor temperature considered over a day for analysis.

Table 2. Data for residential appliances.

Appliances	T_{start} (h)	T_{end} (h)	Power (watt)	Duration of Operation (h)
Interruptible Appliance 1	9	24	1500	3
Interruptible Appliance 2	5	18	2000	4
Deferrable Appliance 1	12	22	1000	4
Deferrable Appliance 2	5	24	2000	3

Table 3. Parameters for thermostatically controlled appliance, battery, and fuel cell plant.

Parameter	Value/Unit
T_{in}^{min}, T_{in}^{max}	24, 26, °C
The initial temperature of the room	20, °C
P_{ch}^{max}, P_{dch}^{max}	5, 5, KW
η_{ch}, η_{dch}	0.9, 0.9, %
SOC_{min}, SOC_{max}	0.3, 0.9, p.u
Minimum and the maximum power that can be supplied from the electric grid	0, 10, kW
Battery volume	6.86, kW
Natural gas cost	0.4, RMB/kW
Maximum limit of power generated by the fuel cell	4, kW
$\Delta P_{FC,U}$, $\Delta P_{FC,D}$	1.5, kW
Maximum limit of power generated by gas	2, kW

Table 4. Must-run electric demand, must-run thermal demand, and real-time electricity price.

Interval (h)	Must-Run Electric Demand (kW)	Must-Run Thermal Demand (kW)	Real-Time Electricity Price (RMB ¥)	Interval (h)	Must-Run Electric Demand (kW)	Must-Run Thermal Demand (kW)	Real-Time Electricity Price (RMB ¥)
1	0.35	1.23	0.21	13	0.48	1.74	0.51
2	0.31	1.34	0.39	14	0.49	1.45	0.41
3	0.30	1.51	0.32	15	0.48	1.40	0.50
4	0.34	1.49	0.49	16	0.71	1.83	0.61
5	0.35	1.47	0.41	17	1.00	3.00	0.71
6	0.41	1.83	0.80	18	2.21	2.98	0.79
7	0.48	2.00	0.71	19	2.80	2.81	0.71
8	1.11	2.15	0.84	20	2.69	2.62	0.61
9	1.12	2.21	0.82	21	1.91	2.89	0.55
10	1.00	2.53	0.71	22	1.20	2.74	0.51
11	0.60	1.57	0.61	23	0.80	1.43	0.41
12	0.49	1.55	0.56	24	0.49	1.36	0.31

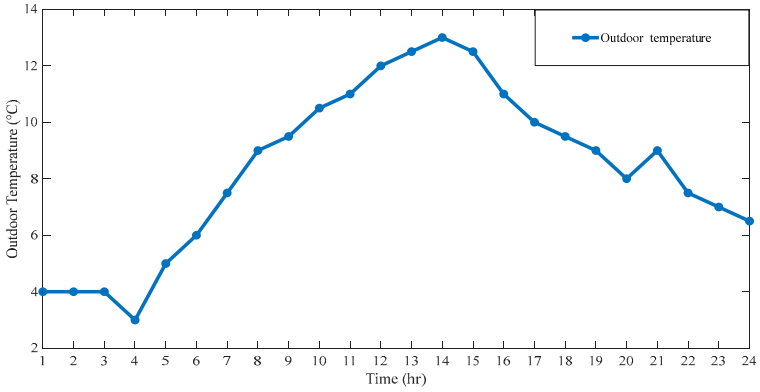

Figure 4. Outdoor Temperature.

For the solution of such a complicated constrained optimization problem, MATLAB 2019 environment was used. The optimization problem was solved using the proposed CAO and AO [41]. The simulation analysis was carried out on a CPU configured with an i5 processor having 4 GB of RAM operated at 1.7 GHz of clock speed.

AO has two major control parameters, α *and* δ, which help to adjust the exploitation process during optimization. The effect of the population (NP), α, and δ are analyzed, with variation in NP from 50 to 200 with its step increment of 50, and with and a step increment of 0.4 for α and δ between 0.1 and 0.9. After analyzing the objective function over thirty repeated trials, statistical results are tabulated as given in Table 5, where it can be observed that with NP = 150, $\alpha = 0.1$, *and* $\delta = 0.1$, AO was able to attain 38.7016 (RMB) as the minimum operational cost with a standard deviation (SD) of 0.8435, which is considered as best control parameters for further analysis. Considering the average computational time, it is observed that it also increases as the population size increases.

To investigate the effect of chaotic sequence, further analysis on the same problem was carried out with AO embedded with a sinusoidal chaotic map.

After performing similar simulation analysis over thirty trials, statistical results in the form of min cost, ave cost, max cost, SD, and ave CPU time are tabulated in Table 6. Here, it is observed that min cost and ave cost improve; however, max cost, SD, and ave CPU time slightly increase. This may be due to the additional randomness of the chaotic sequence. Figure 5 compares the cost convergence curve obtained using AO and CAO over 500 iterations. Here, it is observed that the curve rapidly decreases towards global minima due to the unique and strong exploitation characteristics of AO.

The operational costs obtained by the proposed method and the reported methods are compared in Figure 6. It clearly shows that CAO is able to produce the best solution in terms of cost as 37.221 (RMB) as compared to 38.7016 (RMB) obtained by AO and 43.68 (RMB) by Hybrid CONOPT with PSO [31] and 54.4839 by PSO [30].

The optimal results in terms of power drawn from the battery, fuel cell, grid, and power consumption of must-run electric, thermostatically controlled, deferrable, and interruptible appliances are presented in Tables 7 and 8. These results are corresponding to the best cost obtained by CAO and AO. Considering the power-sharing between different resources, it is evident that the power balance constraints as in (2) are fully satisfied.

Table 5. Effect of Control Parameters of AO on Operational cost.

NP	α	δ	Min Cost (RMB)	Avg. Cost (RMB)	Max Cost (RMB)	SD	Avg. CPU Time (s)
50	0.1	0.1	39.9335	41.8039	44.8229	1.3720	0.0296
		0.5	39.1878	42.4136	44.6321	1.6631	0.0294
		0.9	39.5802	42.8461	44.0489	1.2963	0.0287
	0.5	0.1	40.6965	41.7563	43.6728	1.3456	0.0283
		0.5	41.9451	42.5463	44.5559	1.2345	0.0274
		0.9	42.1972	42.9657	44.9562	1.1456	0.0245
	0.9	0.1	40.7976	42.4673	44.5444	1.3467	0.0265
		0.5	40.6244	42.3667	44.9903	1.2514	0.0243
		0.9	40.8085	42.4566	45.2061	1.1345	0.0275
100	0.1	0.1	38.8224	40.9666	43.2639	1.3493	0.0552
		0.5	39.9459	41.6502	43.4395	1.0668	0.0532
		0.9	40.2902	42.0940	43.7440	0.9640	0.0555
	0.5	0.1	40.2562	41.0034	43.3675	1.2345	0.0532
		0.5	39.6843	41.6654	43.5647	1.2243	0.0534
		0.9	40.3672	41.9653	43.8965	1.0764	0.0565
	0.9	0.1	39.5648	41.1223	43.4362	1.3532	0.0552
		0.5	41.3396	41.6754	43.5784	0.9237	0.0557
		0.9	41.0133	41.9765	43.9564	0.9043	0.0550
150	0.1	0.1	38.7016	40.7247	41.7779	0.8435	0.0854
		0.5	39.2770	40.8556	42.3374	1.1482	0.0788
		0.9	39.5155	41.4336	44.1282	1.2556	0.0783
	0.5	0.1	39.2413	40.9675	42.7654	1.2456	0.0843
		0.5	40.6953	40.9667	43.6573	1.2344	0.0782
		0.9	40.9950	41.5674	44.5693	1.1454	0.0833
	0.9	0.1	39.5178	40.9965	42.6754	1.2354	0.0773
		0.5	39.6799	41.0023	43.8765	1.2444	0.0842
		0.9	39.6864	41.6546	44.6745	1.1674	0.0765
200	0.1	0.1	38.7016	40.7058	42.1987	1.0120	0.1041
		0.5	38.7855	40.7394	41.6864	1.0086	0.1036
		0.9	38.9860	41.1340	42.4047	0.8530	0.1047
	0.5	0.1	39.0991	40.8045	42.3567	0.8765	0.1029
		0.5	39.0056	40.2345	42.4567	0.9875	0.1079
		0.9	39.3174	41.2345	43.5685	1.2223	0.1065
	0.9	0.1	38.7546	40.3456	43.5745	0.9546	0.1042
		0.5	39.0607	41.4450	43.6574	1.1576	0.1075
		0.9	40.0895	41.4567	44.6574	1.1664	0.0993

Table 6. Effect of CAO on Operational cost.

NP	α	δ	Min Cost (RMB)	Avg Cost (RMB)	Max Cost (RMB)	SD	Avg. CPU Time (s)
150	0.1	0.1	37.221	40.0785	41.9972	1.1223	0.0882

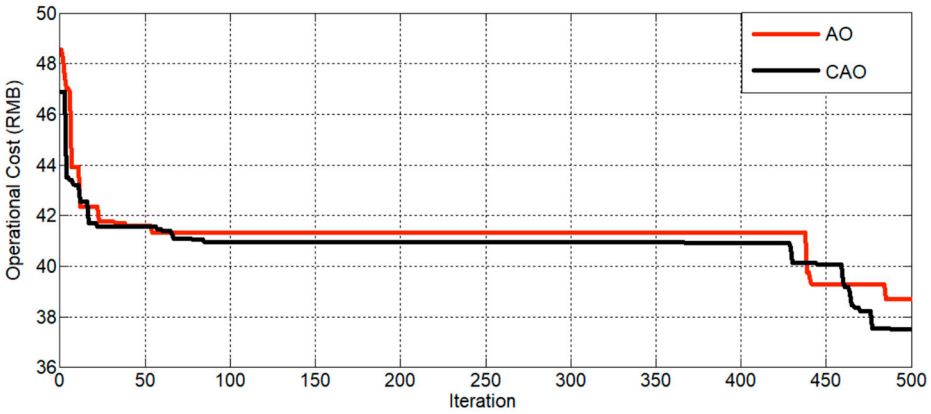

Figure 5. Comparison of Convergence curve for demand response using AO and CAO.

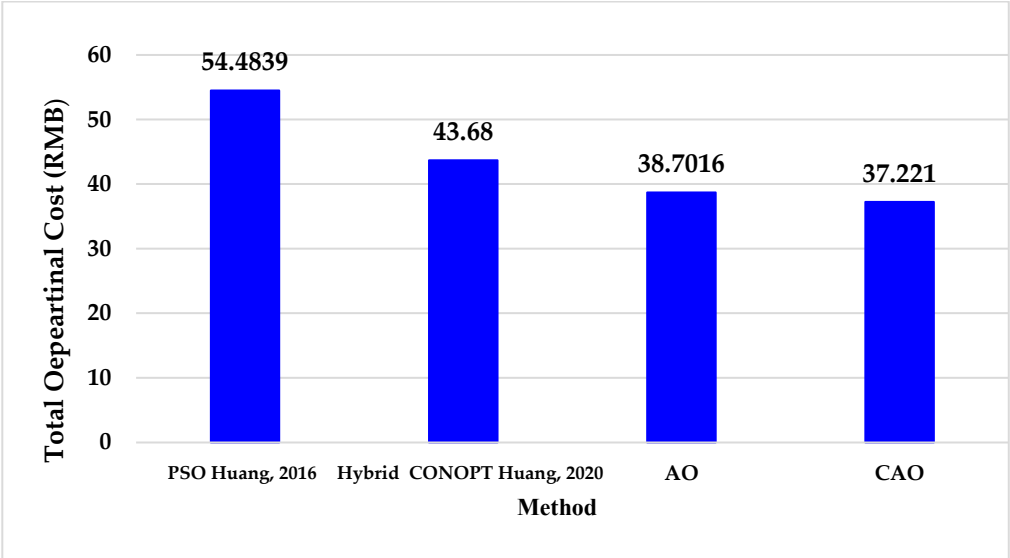

Figure 6. Comparison of operational cost [30,31].

It is noted that the battery is charging when the price of electricity is low and gets discharged to match the required load demand when the electricity price is higher. The positive values of battery power represent the charging, and the negative values indicate the discharging mode of battery status as shown in Tables 7 and 8. Moreover, the SOC is maintained within the limits given in Table 2 over the 24 h interval in an optimal manner. Here, it can be observed that the fuel cell operates within its specified operational constraints and shares more power to limit the use of more expensive grid-available power. All fuel cell constraints are satisfied as given in (17)–(22) as the ramp rate of the fuel cell and the power derived from the fuel cell are within the limits given in Table 2. Hence, the battery and fuel cell simultaneously help in minimizing the cost incurred to the consumers.

The price of electricity is high during intervals 8 to 10. In this duration, fuel cell and battery take turns to fulfill the major power demand of the residential building to reduce the cost of operation. The optimal power sharing between the grid, fuel cell, and battery for over 24 h is presented in Figures 7 and 8 for CAO and AO, respectively.

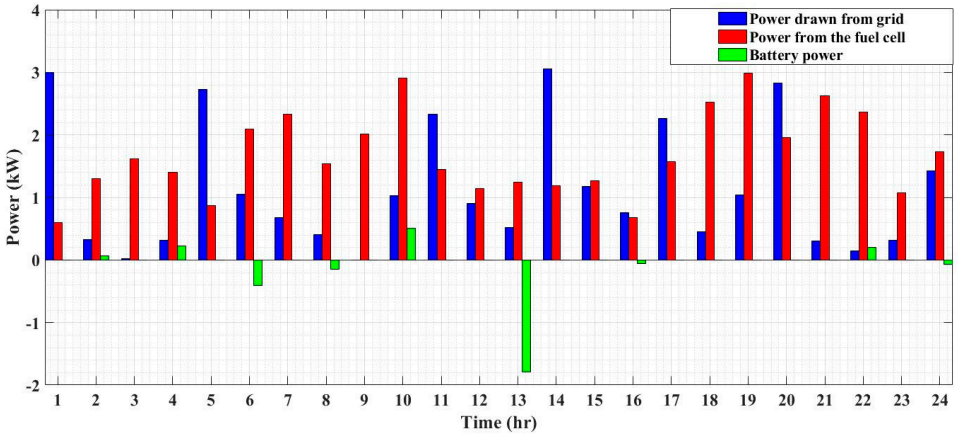

Figure 7. Optimal power sharing between grid, fuel cell, and battery (CAO).

Table 7. Power drawn from the battery, fuel cell, grid, and power consumption of must-run electric, thermostatically controlled, deferrable, and interruptible appliances (CAO).

Interval (h)	p_{batt} (kW)	P_{eFC} (kW)	p_{grid} (kW)	p_{ms} (kW)	p_{td} (kW)	p_{defe} (kW)	p_{inte} (kW)
1	0.0000	0.5992	2.9955	0.350	3.2446	0	0
2	0.0673	1.2959	0.3320	0.310	1.2506	0	0
3	0.0000	1.6197	0.0166	0.300	1.3363	0	0
4	0.2297	1.4063	0.3114	0.340	1.1480	0	0
5	0.0000	0.8743	2.7314	0.350	1.2557	2	0
6	−0.4130	2.0909	1.0540	0.410	1.1479	2	0
7	0.0000	2.3297	0.6761	0.480	0.5259	2	0
8	−0.1527	1.5427	0.4061	1.110	0.9914	0	0
9	0.0000	2.0125	0.0017	1.120	0.8942	0	0
10	0.5041	2.9084	1.0302	1.000	0.4345	0	2
11	0.0000	1.4491	2.3303	0.600	1.1793	0	2
12	0.0000	1.1430	0.9062	0.490	0.5592	1	0
13	−1.7916	1.2400	0.5224	0.480	0.5740	1	1.5
14	0.0000	1.1881	3.0584	0.490	0.7565	1	2
15	−0.0065	1.2611	1.1759	0.480	0.9635	1	0
16	−0.0634	0.6798	0.7583	0.710	0.7915	0	0
17	0.0000	1.5710	2.2586	1.000	0.8295	0	2
18	0.0000	2.5272	0.4565	2.210	0.7737	0	0
19	0.0000	2.9858	1.0447	2.800	1.2305	0	0
20	0.0000	1.9547	2.8259	2.690	0.5906	0	1.5
21	0.0000	2.6293	0.3070	1.910	1.0263	0	0
22	0.1993	2.3651	0.1428	1.200	1.1085	0	0
23	0.0000	1.0788	0.3131	0.800	0.5919	0	0
24	−0.0649	1.7263	1.4214	0.499	1.2135	0	1.5

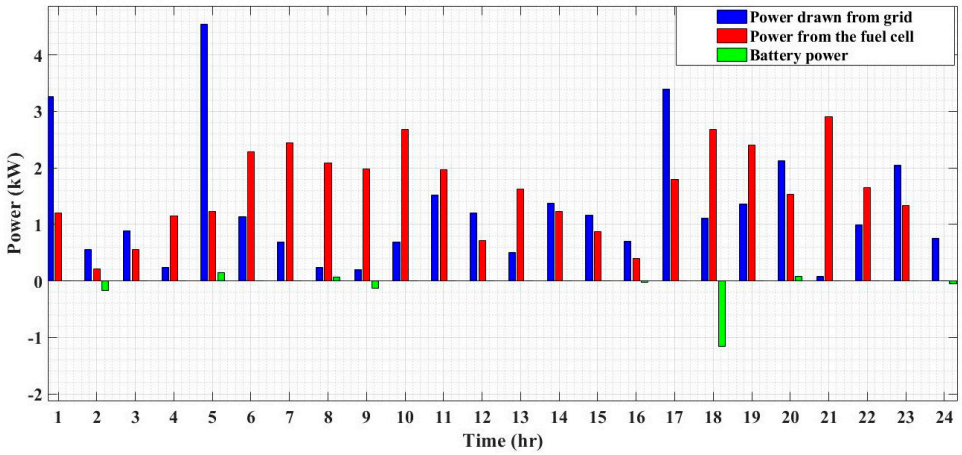

Figure 8. Optimal power sharing between grid, fuel cell, and battery (AO).

Table 8. Power drawn from the battery, fuel cell, grid, and power consumption of must-run electric, thermostatically controlled, deferrable, and interruptible appliances (AO).

Interval (h)	p_{batt} (kW)	P_{eFC} (kW)	p_{grid} (kW)	p_{ms} (kW)	p_{td} (kW)	p_{defe} (kW)	p_{inte} (kW)
1	0.0000	1.1972	3.2582	0.350	4.1054	0	0.0
2	−0.1766	0.2086	0.5538	0.310	0.6290	0	0.0
3	0.0000	0.5497	0.8902	0.300	1.1399	0	0.0
4	0.0000	1.1484	0.2449	0.340	1.0533	0	0.0
5	0.1511	1.2260	4.5431	0.350	1.2680	2	2.0
6	0.0000	2.2850	1.1309	0.410	1.0059	2	0.0
7	0.0000	2.4432	0.6916	0.480	0.6548	2	0.0
8	0.0627	2.0829	0.2347	1.110	1.1449	0	0.0
9	−0.1374	1.9818	0.2052	1.120	1.2044	0	0.0
10	0.0000	2.6836	0.6813	1.000	0.8650	0	1.5
11	0.0000	1.9657	1.5234	0.600	0.8892	0	2.0
12	0.0000	0.7139	1.2094	0.490	0.4333	1	0.0
13	0.0000	1.6241	0.4970	0.480	0.6412	1	0.0
14	0.0000	1.2323	1.3786	0.490	1.1209	1	0.0
15	0.0000	0.8785	1.1674	0.480	0.5659	1	0.0
16	−0.0220	0.3970	0.7067	0.710	0.4157	0	0.0
17	0.0000	1.8037	3.4000	1.000	0.7036	0	3.5
18	−1.1556	2.6810	1.1169	2.210	0.7436	0	2.0
19	0.0000	2.3997	1.3634	2.800	0.9630	0	0.0
20	0.0806	1.5309	2.1246	2.690	0.8849	0	0.0
21	0.0000	2.9050	0.0785	1.910	1.0735	0	0.0
22	0.0000	1.6525	0.9889	1.200	1.4414	0	0.0
23	0.0000	1.3354	2.0475	0.800	1.0829	0	1.5
24	−0.0509	0.0000	0.7478	0.499	0.2997	0	0.0

As specified in Table 1, the distinct appliances connected in the building have specified start–end operational window, minimum operational time, and power consumed by the particular appliances. The electricity tariff rate is dynamically varying with time as shown

in Table 3. For this complicated constrained duration, AO and CAO were also successfully able to optimally schedule the appliances of the building in the most economical manner. Figures 9 and 10 exhibit these scheduling results, respectively. It can be seen that the interruptible appliances do not run continuously and are distributed over the given time interval to reduce the peak load and energy cost, whereas the deferrable appliances run continuously until the task is completed.

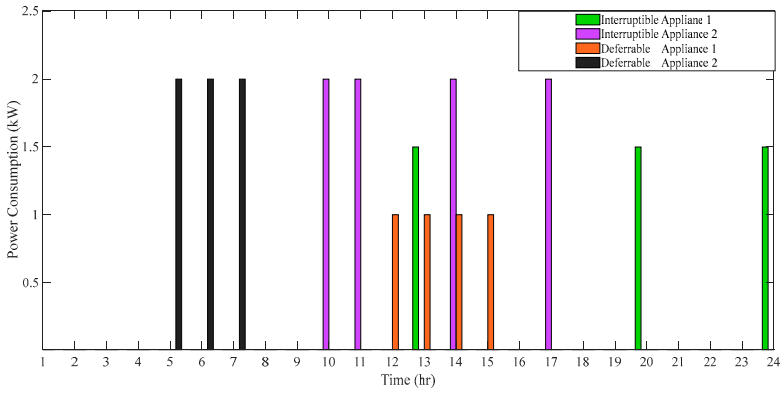

Figure 9. Optimal power consumption pattern for interruptible and deferrable appliances (CAO).

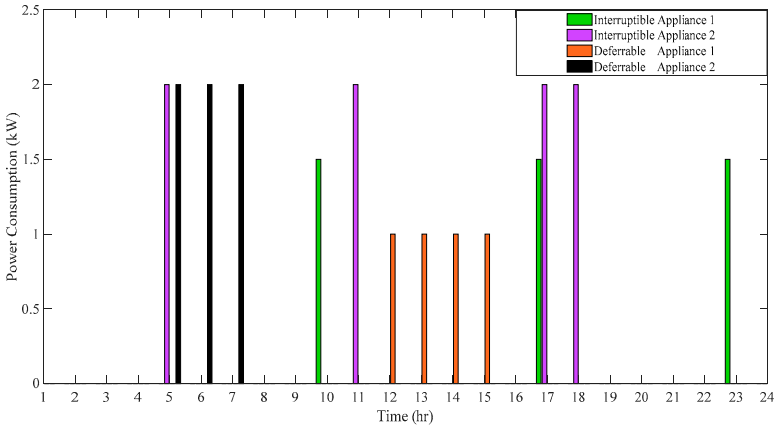

Figure 10. Optimal power consumption pattern for interruptible and deferrable appliances (AO).

The building is also equipped with a thermostatically controlled appliance to control the indoor room temperature. It has to control the temperature within its specified operating temperature range as specified in Table 2. These constraints are also handled by the AO and CAO efficiently. Figure 11 shows the resulting optimal indoor temperatures are within the specified comfort temperature range of the consumer 24–26 °C. The power consumption in maintaining indoor temperature by appliances is presented in Figure 12. It can be seen that if the difference between the outdoor temperature and indoor temperature is greater, then the power consumed by the thermostatically controlled appliance is also greater. Moreover, more power is consumed during the initial operational hour as it had to increase the temperature from 20°C to the desired range. Thereafter, as the temperature reaches the desired range, the temperature and the power consumed become stable.

The thermal power generated by natural gas and fuel cell and the total thermal demand as per the optimal scheduling obtained by AO and CAO are compared in Table 9 below. There, it is also observed that the operational constraint as specified in (3) is also satisfied.

Table 9. Total thermal demand and thermal power generated by natural gas and fuel cell.

Interval (h)	P_{hms} (kW)	P_{gas} (kW)	P_{hFC} (kW)	P_{gas} (kW)	P_{hFC} (kW)
		CAO		AO	
1	1.23	0.8290	0.4010	0.4041	0.8259
2	1.34	0.4393	0.9007	1.1996	0.1404
3	1.51	0.3535	1.1565	1.1423	0.3677
4	1.49	0.5039	0.9861	0.7006	0.7894
5	1.47	0.8791	0.5909	0.6225	0.8475
6	1.83	0.2712	1.5588	0.0938	1.7362
7	2.00	0.2218	1.7782	0.1132	1.8868
8	2.15	1.0558	1.0942	0.5983	1.5517
9	2.21	0.7208	1.4892	0.7478	1.4622
10	2.53	0.1584	2.3716	0.4016	2.1284
11	1.57	0.5504	1.0196	0.1218	1.4482
12	1.55	0.7646	0.7854	1.0708	0.4792
13	1.74	0.8819	0.8581	0.5799	1.1601
14	1.45	0.6309	0.8191	0.5977	0.8523
15	1.40	0.5259	0.8741	0.8061	0.5939
16	1.83	1.3742	0.4558	1.5644	0.2656
17	3.00	1.8831	1.1169	1.6909	1.3091
18	2.98	1.0106	1.9694	0.8543	2.1257
19	2.81	0.3498	2.4602	0.9652	1.8448
20	2.62	1.1814	1.4386	1.5353	1.0847
21	2.89	0.8177	2.0723	0.5223	2.3677
22	2.74	0.9283	1.8117	1.5567	1.1833
23	1.43	0.6919	0.7381	0.4990	0.9310
24	1.36	0.1158	1.2442	1.3600	0.0000

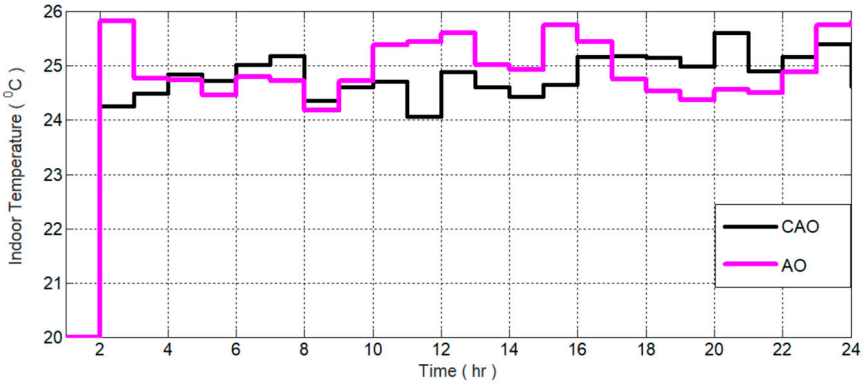

Figure 11. Optimal Indoor Temperature (CAO and AO).

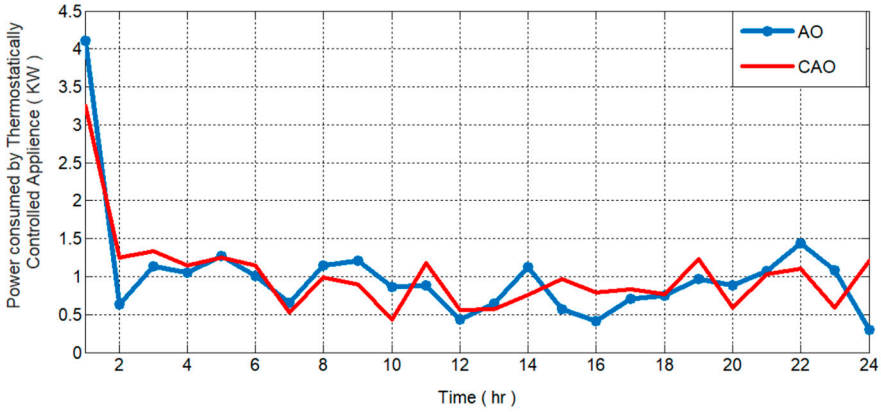

Figure 12. Power consumption of thermostatically controlled appliances (AO and CAO).

5. Conclusions and Future Work

In this paper, Chaotic Aquila Optimization (CAO) is proposed for the solution of a DR program for a GCRMG system. The optimal scheduling of connected appliances has been carried out considering operational constraints such as variable electricity tariffs, customer comfort, and limitations of the distinct power resources. Obtained simulation results reveal the better searching capability of AO due to its unique exploration and exploitation phase and strong constrained handling capability. A comparison of results obtained by AO is found to be superior than the reported results using PSO [30] and a hybrid algorithm using CONOPT and PSO [31]. In addition, experimental results show a sinusoidal map that significantly improves the performances of AO.

The MG system provides flexibility in deploying DER for improving the voltage stability of the overall system. Integrating wind turbines and solar PV systems helps to resolve environmental problems and also depletion of conventional resources. The power flow model is not considered in the paper, and to make the DR program more realistic, we could get an idea from [13,47]. Future work may include: (i) RES integration with BSS, (ii) inclusion of electric load as electric vehicle charging, and (iii) optimal power flow with the dynamic form of DR.

Author Contributions: Conceptualization, S.K., S.R.S. and H.M.D.; methodology, S.R.S. and H.M.D.; software, S.K. and S.R.S.; validation, S.K., H.M.D. and S.R.S.; formal analysis, S.R.S.; investigation, S.K.; resources, H.M.D. and S.R.S.; data curation, S.K.; writing—original draft preparation, S.K., S.R.S. and H.M.D.; writing—review and editing, H.M.D. and S.R.S.; visualization, S.K.; supervision, H.M.D. and S.R.S.; project administration, S.K. and H.M.D.; funding acquisition, S.R.S. and H.M.D. All authors have read and agreed to the published version of the manuscript.

Funding: This research was funded by "Woosong University's Academic Research Funding—2023".

Institutional Review Board Statement: Not applicable.

Informed Consent Statement: Not applicable.

Data Availability Statement: Not applicable.

Conflicts of Interest: The authors declare no conflict of interest.

Nomenclature

F_{min}	Minimum cost (RMB)	$P_{hms}(h)$	total thermal consumption (kW)
h	Time step (h)	p_{ch}^{max}, p_{dch}^{max}	Battery maximum charging and discharging power (kW)
$T_{elec}(h)$	Hourly electricity price (RMB)	η_{ch},η_{dch}	Battery charging and discharging efficiency (%)
$p_{grid}(h)$	quantity of power traded with the utility grid (kW)	$SOC(h)$	Battery's state of charge (p.u.)
T_{gas}	Cost of natural gas (RMB/kW)	T_{in} (h)	Inside temperature (°C)
$p_{gas}(h)$	heat power generated by natural gas (kW)	$T_{out}(h)$	Outside temperature (°C)
$P_{FC}(h)$	total power of the fuel cell (kW)	δ	switching state of appliance: 1 for ON; 0 for OFF.
$p_{batt}(h)$	Battery power (kW)	H	Time slot (h)
$p_{eFC}(h)$	Electrical power of fuel cell (kW)	α_a, β_a	Working time range of electrical appliance. (h)
E_{batt}	Battery capacity (kW)	$\Delta P_{FC,U}$	Upper limit of a fuel cell's ramp rate. (kW)
$p_{ms}(h)$	total energy used by unscheduled, must-run electrical appliances (kW)	$\Delta P_{FC,D}$	Lower limit of a fuel cell's ramp rate. (kW)
$p_{defe}(h)$	power consumed by deferrable appliances (kW)	$P_{FC,min}$	Minimum limit for power generated by the fuel cell (kW)
$p_{inte}(h)$	power consumed by interruptible appliances (kW)	$P_{FC,max}$	Maximum limit for power generated by the fuel cell (kW)
$p_{td}(h)$	power usage of a thermostatically controlled appliance (kW)	$p_{batt}^{ch}(h)$, p_{batt}^{dch} (h)	Battery charging and discharging power (KW)
$P_{hFC}(h)$	heat power generated by the fuel cell (kW)		

References

1. Fang, X.; Misra, S.; Xue, G.; Yang, D. Smart grid-The new and improved power grid: A survey. *IEEE Commun. Surv. Tutor.* **2012**, *14*, 944–980. [CrossRef]
2. Salkuti, S.R. Emerging and Advanced Green Energy Technologies for Sustainable and Resilient Future Grid. *Energies* **2022**, *15*, 6667. [CrossRef]
3. Varaiya, P.P.; Wu, F.F.; Bialek, J.W. Smart operation of smart grid: Risk-limiting dispatch. *Proc. IEEE* **2011**, *99*, 40–57. [CrossRef]
4. Golmohamadi, H. Demand-Side Flexibility in Power Systems: A Survey of Residential, Industrial, Commercial, and Agricultural Sectors. *Sustainability* **2022**, *14*, 7916. [CrossRef]
5. Connell, N.O.; Pinson, P.; Madsen, H.; O'Malley, M.O. Benefits and challenges of electrical demand response: A critical review. *Renew. Sustain. Energy Rev.* **2014**, *39*, 686–699. [CrossRef]
6. Jordehi, A.R. Optimisation of demand response in electric power systems, a review. *Renew. Sustain. Energy Rev.* **2019**, *103*, 308–319. [CrossRef]
7. Pedrasa, M.A.A.; Spooner, T.D.; MacGill, I.F. Coordinated Scheduling of Residential Distributed Energy Resources to Optimize Smart Home Energy Services. *IEEE Trans. Smart Grid* **2010**, *1*, 134–143. [CrossRef]
8. Nwulu, N.I.; Xia, X. Optimal dispatch for a microgrid incorporating renewables and demand response. *Renew. Energy* **2017**, *101*, 16–28. [CrossRef]
9. Dubey, S.M.; Dubey, H.M.; Pandit, M. Incentive-based demand response in grid-connected microgrid using quasi-opposed grey wolf optimizer. *Int. J. Eng. Sci. Technol.* **2021**, *13*, 1–14. [CrossRef]
10. Astriani, Y.; Shafiullah, G.M.; Shahnia, F. Incentive determination of a demand response program for microgrids. *Appl. Energy* **2021**, *292*, 116624. [CrossRef]
11. Hassan, M.A.S.; Assad, U.; Farooq, U.; Kabir, A.; Khan, M.Z.; Bukhari, S.S.H.; Jaffri, Z.u.A.; Oláh, J.; Popp, J. Dynamic Price-Based Demand Response through Linear Regression for Microgrids with Renewable Energy Resources. *Energies* **2022**, *15*, 1385. [CrossRef]
12. Harsh, P.; Das, D. Energy management in microgrid using incentive-based demand response and reconfigured network considering uncertainties in renewable energy sources. *Sustain. Energy Technol. Assess.* **2021**, *46*, 101225. [CrossRef]
13. Yao, M.; Molzahn, D.K.; Mathieu, J.L. An Optimal Power-Flow Approach to Improve Power System Voltage Stability Using Demand Response. *IEEE Trans. Control Netw. Syst.* **2019**, *6*, 1015–1025. [CrossRef]
14. Monfared, H.J.; Ghasemi, A.; Loni, A.; Marzband, M. A hybrid price-based demand response program for the residential micro-grid. *Energy* **2019**, *185*, 274–285. [CrossRef]
15. Zhang, Z.; Huang, Y.; Chen, H.; Huang, Q.; Lee, W.J. A Novel Hierarchical Demand Response Strategy for Residential Microgrid. *IEEE Trans. Ind. Appl.* **2021**, *57*, 3262–3271. [CrossRef]
16. Hosseini, S.M.; Carli, R.; Dotoli, M. Robust Day-ahead Energy Scheduling of a Smart Residential User under Uncertainty. In Proceedings of the 18th European Control Conference (ECC 2019), Naples, Italy, 25–28 June 2019; pp. 935–940. [CrossRef]

17. Dayalan, S.; Gul, S.S.; Rathinam, R.; Fernandez Savari, G.; Aleem, S.H.E.A.; Mohamed, M.A.; Ali, Z.M. Multi-Stage Incentive-Based Demand Response Using a Novel Stackelberg–Particle Swarm Optimization. *Sustainability* **2022**, *14*, 10985. [CrossRef]
18. Sanjari, M.J.; Karami, H.; Yatim, A.H.; Gharehpetian, G.B. Application of hyper-spherical search algorithm for optimal energy resources dispatch in residential microgrids. *Appl. Soft Comput.* **2015**, *37*, 15–23. [CrossRef]
19. Zhang, C.; Xu, Y.; Dong, Z.Y.; Wong, K.P. Robust Coordination of Distributed Generation and Price-Based Demand Response in Microgrids. *IEEE Trans. Smart Grid* **2018**, *9*, 4236–4247. [CrossRef]
20. Pothireddy, K.M.R.; Vuddanti, S.; Salkuti, S.R. Impact of Demand Response on Optimal Sizing of Distributed Generation and Customer Tariff. *Energies* **2022**, *15*, 190. [CrossRef]
21. Jin, M.; Feng, W.; Liu, P.; Marnay, C.; Spanos, C. MOD-DR: Microgrid optimal dispatch with demand response. *Appl. Energy* **2017**, *187*, 758–776. [CrossRef]
22. Li, Y.; Li, K.; Yang, Z.; Yu, Y.; Xu, R.; Yang, M. Stochastic optimal scheduling of demand response-enabled microgrids with renewable generations: An analytical-heuristic approach. *J. Clean. Prod.* **2022**, *330*, 129840. [CrossRef]
23. Tiwari, V.; Dubey, H.M.; Pandit, M.; Salkuti, S.R. CHP-Based Economic Emission Dispatch of Microgrid Using Harris Hawks Optimization. *Fluids* **2022**, *7*, 248. [CrossRef]
24. Karami, H.; Sanjari, M.J.; Hosseinian, S.H.; Gharehpetian, G.B. An Optimal Dispatch Algorithm for Managing Residential Distributed Energy Resources. *IEEE Trans. Smart Grid* **2014**, *5*, 2360–2367. [CrossRef]
25. Habib, H.U.R.; Wang, S.; Waqar, A.; Farhan, B.S.; Kotb, K.M.; Kim, Y.S. Combined Heat and Power Units Sizing and Energy Cost Optimization of a Residential Building by Using an Artificial Bee Colony Algorithm. *IEEE Access* **2020**, *8*, 218289–218303. [CrossRef]
26. Wang, Y.; Huang, Y.; Wang, Y.; Zeng, M.; Li, F.; Wang, Y.; Zhang, Y. Energy management of smart micro-grid with response loads and distributed generation considering demand response. *J. Clean. Prod.* **2018**, *197*, 1069–1083. [CrossRef]
27. Yu, Z.X.; Li, M.S.; Xu, Y.P.; Aslam, S.; Li, Y.K. Techno-Economic Planning and Operation of the Microgrid Considering Real-Time Pricing Demand Response Program. *Energies* **2021**, *14*, 4597. [CrossRef]
28. da Silva, I.R.S.; Rabelo, A.L.R.D.; Rodrigues, J.J.P.C.; Solic, P.; Carvalho, A. A preference-based demand response mechanism for energy management in a microgrid. *J. Clean. Prod.* **2020**, *255*, 120034. [CrossRef]
29. Gamil, M.M.; Ueda, S.; Nakadomari, A.; Konneh, K.V.; Senjyu, T.; Hemeida, A.M.; Lotfy, M.E. Optimal Multi-Objective Power Scheduling of a Residential Microgrid Considering Renewable Sources and Demand Response Technique. *Sustainability* **2022**, *14*, 13709. [CrossRef]
30. Huang, Y.; Wang, L.; Kang, Q.; Wu, Q. Model predictive control-based demand response for optimization of residential energy consumption. *Electr. Power Compon. Syst.* **2016**, *44*, 1177–1187. [CrossRef]
31. Huang, Y.; Zhang, J.; Mo, Y.; Lu, S.; Ma, J. A Hybrid Optimization Approach for Residential Energy Management. *IEEE Access* **2020**, *8*, 225201–225209. [CrossRef]
32. Hemmati, M.; Mirzaei, M.A.; Abapour, M.; Zare, K.; Mohammadi-ivatloo, B.; Mehrjerdi, H.; Marzband, M. Economic-environmental analysis of combined heat and power-based reconfigurable microgrid integrated with multiple energy storage and demand response program. *Sustain. Cities Soc.* **2021**, *69*, 102790. [CrossRef]
33. Fleschutz, M.; Bohlayer, M.; Braun, M.; Murphy, M.D. Demand Response Analysis Framework (DRAF): An Open-Source Multi-Objective Decision Support Tool for Decarbonizing Local Multi-Energy Systems. *Sustainability* **2022**, *14*, 8025. [CrossRef]
34. Tabar, V.S.; Ghassemzadeh, S.; Tohidi, S. Energy management in hybrid microgrid with considering multiple power market and real-time demand response. *Energy* **2019**, *174*, 10–23. [CrossRef]
35. Dranka, G.G.; Ferreira, P. Review and assessment of the different categories of demand response potentials. *Energy* **2019**, *179*, 280–294. [CrossRef]
36. Yan, X.; Ozturk, Y.; Hu, Z.; Song, Y. A review on price-driven residential demand response. *Renew. Sustain. Energy Rev.* **2018**, *96*, 411–419. [CrossRef]
37. Melhem, F.Y.; Grunder, O.; Hammoudan, Z.; Moubayed, N. Energy Management in Electrical Smart Grid Environment Using Robust Optimization Algorithm. *IEEE Trans. Ind. Appl.* **2018**, *54*, 2714–2726. [CrossRef]
38. Dubey, H.M.; Pandit, M.; Panigrahi, B.K. An overview and comparative analysis of recent bio-inspired optimization techniques for wind integrated multi-objective power dispatch. *Swarm Evol. Comput.* **2018**, *38*, 12–34. [CrossRef]
39. Dubey, S.M.; Dubey, H.M.; Salkuti, S.R. Modified Quasi-Opposition-Based Grey Wolf Optimization for Mathematical and Electrical Benchmark Problems. *Energies* **2022**, *15*, 5704. [CrossRef]
40. Wolpert, D.H.; Macready, W.G. No free lunch theorems for optimization. *IEEE Trans. Evol. Comput.* **1997**, *1*, 67–82. [CrossRef]
41. Abualigah, L.; Yousri, D.; Elaziz, M.A.; Ewees, A.A.; Al-Ganess, M.A.A.; Gandomi, A.H. Aquila Optimizer: A novel metaheuristic optimization Algorithm. *Comput. Ind. Eng.* **2021**, *157*, 107250. [CrossRef]
42. Hussan, M.R.; Sarwar, M.I.; Sarwar, A.; Tariq, M.; Ahmad, S.; Shah Noor Mohamed, A.; Khan, I.A.; Ali Khan, M.M. Aquila Optimization Based Harmonic Elimination in a Modified H-Bridge Inverter. *Sustainability* **2022**, *14*, 929. [CrossRef]
43. Abou El-Ela, A.A.; El-Sehiemy, R.A.; Shaheen, A.M.; Shalaby, A.S. Aquila Optimization Algorithm for Wind Energy Potential Assessment Relying on Weibull Parameters Estimation. *Wind* **2022**, *2*, 617–635. [CrossRef]
44. Wang, S.; Jia, H.; Abualigah, L.; Liu, Q.; Zheng, R. An Improved Hybrid Aquila Optimizer and Harris Hawks Algorithm for Solving Industrial Engineering Optimization Problems. *Processes* **2021**, *9*, 1551. [CrossRef]

45. Mirjalili, S.; Gandomi, A.H. Chaotic gravitational constants for the gravitational search algorithm. *Appl. Soft Comput.* **2017**, *53*, 407–419. [CrossRef]
46. Sayed, G.I.; Hassanien, A.E.; Azar, A.T. Feature selection via a novel chaotic crow search algorithm. *Neural Comput. Appl.* **2019**, *31*, 171–188. [CrossRef]
47. Scarabaggio, P.; Carli, R.; Dotoli, M. Noncooperative Equilibrium-Seeking in Distributed Energy Systems Under AC Power Flow Nonlinear Constraints. *IEEE Trans. Control Netw. Syst.* **2022**, *9*, 1731–1742. [CrossRef]